รายงานวิจัยฉบับสมบูรณ์

สังเกตการณ์รัศมีคู่อิเล็กตรอน/โพสิตรอนด้วยรังสีเอ็กซ์

โดย

ดร. อนันต์ อึ้งวณิชยพันธ์

กรกฎาคม 2554

สัญญาเลขที่ MRG5080345

รายงานวิจัยฉบับสมบูรณ์

สังเกตการณ์รัศมีคู่อิเล็กตรอน/โพสิตรอนด้วยรังสีเอ็กซ์

โดย

ดร. อนันต์ อึ้งวณิชยพันธ์

มหาวิทยาลัยแม่ฟ้าหลวง

สนับสนุนโดยสำนักงานคณะกรรมการการอุดมศึกษาและสำนักงานกองทุนสนับสนุนการวิจัย

(ความเห็นในรายงานนี้เป็นของผู้วิจัย สกอ. และ สกว. ไม่จำเป็นต้องเห็นด้วยเสมอไป)

กิตติกรรมประกาศ

ผู้วิจัยขอขอบคุณสำนักงานคณะกรรมการการอุดมศึกษา (สกอ.) และสำนักงานกองทุนสนับสนุนการวิจัย (สกว.) ที่ให้การสนับสนุนเงินทุนการวิจัยตลอดโครงการวิจัย ขอขอบพระคุณ ศาสตราจารย์ ดร. เดวิด รูฟโฟโล นักวิจัยที่ปรึกษาในโครงการ ที่ให้คำปรึกษาอันมีค่าจนงานวิจัยนี้สำเร็จได้ด้วยดี ขอขอบคุณ ดร.อเลฮานโดร ซาอิส ในการให้ข้อเสนอแนะที่เป็นประโยชน์ ขอขอบคุณ นางสาววิระพร ไหมทอง นักศึกษาปริญญาเอกที่ช่วยปรับปรุงโปรแกรมเพื่อคำนวณการแจกแจงพลังงานและมุมของรังสีเอ็กซ์ที่มาจากรัศมีคู่อิเล็กตรอน/โพสิตรอน ขอบคุณมหาวิทยาลัยแม่ฟ้าหลวง ที่สนับสนุนสถานที่และอุปกรณ์เครื่องมือในการวิจัย และที่ขาดไม่ได้คือขอขอบคุณ ดร. ประภัสสร อึ้งวณิชยพันธ์ ที่เป็นกำลังใจและสนับสนุนตลอดมา

ผู้ช่วยศาสตราจารย์ ดร. อนันต์ อึ้งวณิชยพันธ์
มหาวิทยาลัยแม่ฟ้าหลวง
2554

บทคัดย่อ

รหัสโครงการ: MRG5080345
ชื่อโครงการ: สังเกตการณ์รัศมีคู่อิเล็กตรอน/โพสิตรอนด้วยรังสีเอ็กซ์
ชื่อนักวิจัย: ดร. อนันต์ อึ้งวณิชยพันธ์ สำนักวิชาวิทยาศาสตร์
มหาวิทยาลัยแม่ฟ้าหลวง
Email address: a.eungwanichayapant@sci.mfu.ac.th
ระยะเวลาโครงการ: 1 กรกฎาคม 2550 ถึง 30 มิถุนายน 2554

การศึกษารัศมีคู่อิเล็กตรอน/โพสิตรอนที่ผ่านมาเป็นการศึกษาผ่านรังสีแกมม่าที่ถูกสร้างขึ้นโดยกระบวนการ inverse Compton scattering ของอิเล็กตรอนและโพสิตรอนที่กระจายตัวอยู่รอบๆ Active Galactic Nuclei (AGN) ซึ่งเป็นแหล่งกำเนิดรังสีแกมม่าพลังงานสูง (E > 100 GeV) ที่เป็นตัวเกระตุ้นให้เกิดกระบวนการ electromagnetic cascades อันเป็นสาเหตให้เกิดรัศมีคู่รอบๆแหล่งกำเนิดดังกล่าว อันที่จริงแล้วนักฟิสิกส์ดาราศาสตร์อาจจะยังไม่คาดคิดว่าเรายังสามารถศึกษารัศมีคู่ผ่านการแผ่รังสีเอ็กซ์ซึ่งเกิดจาก synchrotron radiation ของคู่อิเล็กตรอน/โพสิตรอนภายใต้สนามแม่เหล็กระหว่างดาราจักรได้ งานวิจัยชิ้นนี้จึงได้ทำการศึกษาการแผ่รังสี synchrotron ของรัศมีคู่โดยการคำนวณหาการแจกแจงพลังงานและระยะทางเชิงมุมของโฟตอน synchrotron ในสถาณการณ์ต่างๆ โดยใช้การวิธี Monte Carlo simulation จากผลการคำนวณที่ได้เราพบว่าเมื่อพลังงานของรังสีแกมม่าจาก AGN เพิ่มมากขึ้น ค่าสุดยอด (peak) ของ Spectral Energy Distribution ของการแผ่รังสี synchrotron จะเพิ่มขึ้น และฟลักซ์จะกระจุกอยู่ตรงใจกลางของรัศมีคู่มากขึ้น เมื่อความเข้มของสนามแม่เหล็กเพิ่มมากขึ้นฟลักซ์ของรังสี synchrotron จะเพิ่มขึ้นแต่ฟลักซ์จะกระจายออกไปในแนวรัศมีมากขึ้นจนกระทั้งสนามแม่เหล็กมากกว่า 1 μG ฟลักซ์จะกลับมากระจุกอยู่ที่ตรงใจกลางเหมือนเดิม

คำสำคัญ: *Very High Energy (VHE) gamma-rays, Intergalactic magnetic field, Electromagnetic cascades, Gamma-rays astronomy, X-ray Astronomy, electron/positron pair halos, Monte Calro simulation*

Abstract

Project code:	MRG5080345
Project title:	Observing electron/positron Pair Halos with X-ray
Investigator:	Dr. Anant Eungwanichayapant, School of Science, Mae Fah Luang University
Email address:	a.eungwanichayapant@sci.mfu.ac.th
Project period:	1 July 2007 to 30 June 2011

The previous electron/positron pair halo studies were based on gamma-rays generated by inverse Compton scattering of electrons and positrons around Active Galactic Nuclei (AGN), which is the source of Very High Energy (VHE, E > 100 GeV) gamma-ray triggering electromagnetic cascades causing the pair halo around the source. Actually, astrophysicist might not consider that we can study the pair halos with X-ray produced via synchrotron radiation of electrons/positrons under intergalactic magnetic field. We study the synchrotron the pair halos by observing the energy and angular distributions computed by Monte Carlo simulation. We found that when the energy of the VHE gamma-ray increased the peak of the synchrotron Spectral Energy Distribution (SED) also increased and the angular distributions were more centrally peak. If the magnetic field strength increased, the synchrotron flux increased too, but the angular distributions were less centrally peak until the magnetic field bigger than 1 μG it back to be more centrally peak again.

Keywords: *Very High Energy (VHE) gamma-rays, Intergalactic magnetic field, Electromagnetic cascades, Gamma-rays astronomy, X-ray Astronomy, electron/positron pair halos, Monte Calro simulation*

Executive Summary

รัศมีคู่อิเล็กตรอน/โพสิตรอนคือปรากฏการณ์ทางธรรมชาติที่เกิดจากการพัฒนาของ electromagnetic cascades ภายใต้สนามแม่เหล็กระหว่างดาราจักร์ทำให้เกิดกลุ่มคู่อิเล็กตรอน/โพสิตรอนกระจายอยู่รอบๆ แหล่งกำเนิดของรังสีแกมม่าพลังงานสูงที่ไปเริ่มต้นกระบวนการ electromagnetic cascades เช่น Active Galactic Nuclei (AGN) คู่อิเล็กตรอน/โพสิตรอนเหล่านี้สามารถแผ่รังสีได้ทั้งในย่านรังสีแกมม่าผ่านกระบวนการ inverse Compton scattering และรังสีเอ็กซ์ผ่านกระบวนการ synchrotron radiation การศึกษาเกี่ยวกับรัศมีคู่ฯที่ผ่านมานักฟิสิกส์ดาราศาสตร์ได้ให้ความสนใจศึกษารัศมีคู่ฯเฉพาะในย่านรังสีแกมม่าเท่านั้น สิ่งนี้สามารถเข้าใจได้เพราะในแบบจำลองแรกๆของรัศมีคู่อิเล็กตรอน/โพสิตรอนได้ทำนายไว้อย่างชัดเจน งานวิจัยชิ้นนี้ได้ปรับปรุงแบบจำลองให้มีความสมบูรณ์มากขึ้นโดยทำการเพิ่มผลกระทบของสนามแม่เหล็กระหว่างดาราจักรต่อ electromagnetic cascades ในแง่ของการแผ่รังสี synchrotron ของคู่อิเล็กตรอน/โพสิตรอน ซึ่งในแบบจำลองแรกๆได้ละเลยไป การศึกษาครั้งนี้เราได้นำการจำลองสถานการณ์โดยใช้เทคนิควิธี Monte Carlo เพื่อติดตามกระบวนการ electromagnetic cascades ทั้งหมดเพื่อเก็บข้อมูลของการแผ่รังสี synchrotron ของอิเล็กตรอนและโพสิตรอนทุกตัวแล้วนำมาคำนวณหาการแจกแจงพลังงานและระยะทางเชิงมุมของโฟตอน synchrotron ที่มาจากรัศมีคู่ การแจกแจงพลังงานและระยะทางเชิงมุมในหลายๆสถานการณ์ อาทิ การปรับเปลี่ยนพลังงานของรังสีแกมม่าพลังงานสูงที่ไปเริ่มต้นกระบวนการ electromagnetic cascades และ การปรับเปลี่ยนความแรงของสนามแม่เหล็กระหว่างดาราจัก ทำให้เราได้เข้าใจธรรมชาติของรัศมีคู่มากขึ้น นอกจากนี้จากผลการคำนวณที่ได้เรายังพบเครื่องมือวัดรังสีเอ็กซ์ที่เรามีในปัจจุบันยังมีความไวต่อการตอบสนอง (sensitivity) สูงกว่าปริมาณฟลักซ์ของรังสี synchrotron จากรัศมีคู่อยู่มาก ในงานวิจัยขั้นถัดไปจะเป็นการนำชุดข้อมูล X-ray ของ AGN ที่มีศักยภาพที่จะให้กำเนิดรัศมีคู่มาวิเคราะห์หาสัญญาณของรัศมีคู่

Contents

List of Figures

Chapter 1

Introduction

A pair halo represents a number of $e^{\pm}$ generated by the developing electromagnetic cascades in an intergalactic (IG) medium (e.g. [1, 2, 3]) around Very High Energy (VHE) gamma-ray sources such as Active Galactic Nuclei (AGN). The cascade in the IG medium is supported by 2 processes: (i) by inverse Compton scattering (IC) on the Cosmic Microwave Background (CMB) photons and (ii) by photon-photon pair production (PP) on Extragalactic Background Light (EBL) (also on CMB for gamma-ray energies above 100 TeV). When the magnetic field near the source is sufficiently large, $B \geq 10^{-9}$ G (generally on the scales of tens of Mpc, but within tens of kpc if the spectrum of primary gamma-rays extends into the PeV region; where PeV $=10^{15}$ eV), i.e., when the mean free path of cascade electrons (at least at the initial stages) is large compared to Larmor radii, the cascade will generate, even for a highly beamed primary source, an extended isotropic pair halo. Therefore, the pair halos are believed that they will unveil the hidden AGNs, especially Blazar, whose jets do not align to the line of sight of the observer on the earth. Another interesting quantities from the pair halos are their spatial and energy distributions. Both distributions of gamma-rays formed during the cascade development in the vicinity of non-thermal extragalactic objects depend on the CIB at the epoch corresponding to the red shift of the central source. Thus, the detection and study of angular and energy distributions of gamma-rays from Pair Halos surrounding extragalactic objects at different red shifts would provide us with unique information about the CIB at remote cosmological epochs and its evolution in time, not achievable by other means. Indeed, the direct measurements of CIB, as well as the derivation of the CIB, based on the study of absorption of gamma-rays in the intergalactic medium, contain information only about the CIB integrated over large cosmological time scales.

X-ray energy band is another window that the pair halos can be observed. Because the intergalactic magnetic field not only gyrate the $e^{\pm}$ pairs but also make the $e^{\pm}$s radiate synchrotron photons, which cover from the visible to X-ray but X-ray is the most promising band if we want to observe the synchrotron pair halos since most of synchrotron energy contain in this band. In this work, we adopted Monte Carlo simulation to compute the energy and angular distribution of the synchrotron photon generated by the pair halos. The computed distributions in difference situations such as the pair halos from difference intrinsic gamma-ray energies and magnetic field strengths, and used them to understand

the nature of the pair halos.

The structure of this report are the following. Chapter 2 give more detail of physical processes in the pair halo model. It also included the detail of all concerned interactions: $\gamma\gamma$ pair production, inverse Compton scattering and synchrotron radiation. The Monte Carlo techniques used in the simulation were in Chapter 3. The results from the simulation and the discussion was presented in Chapter 4.

Chapter 2

Giant Electron-Positron Pair Halos

2.1 Interactions

For the electron-positron ($e^{\pm}$) pair halo model, there are two interactions which are relevant. One is $\gamma\gamma$ pair production (PP), and the other is inverse Compton scattering (IC). In the following, the physics of these interactions are discussed.

Three different inertial frames are used, with primes denoting variables in the electron rest frame, "hats" ($\hat{}$) denoting variables in the center-of-momentum (CM) frame. Otherwise the variables are measured in the lab frame.

Note that only in this section, Sec.2.1, the units $m_e = 1$, $\hbar = 1$ and $c = 1$ are used.

2.1.1 $\gamma\gamma$ Pair Production

From special relativity one obtains the energy condition by applying conservation of four momentum, p_μ, and the invariance of $p_\mu p^\mu$. The result is

$$2(1-\hat{\beta}^2)^{-1} = \varepsilon\omega(1-\cos\theta), \tag{2.1}$$

where ε and ω represent the lab-frame energy of the colliding photons, θ is the angle between their lab-frame 3-momenta, and $\hat{\beta}$ is the speed of $e^{\pm}$ in the CM frame. The threshold condition is derived by assuming that the photons collide head-on and produce an $e^{\pm}$ pair at rest:

$$\varepsilon_{th} = \frac{1}{\omega}. \tag{2.2}$$

Using the standard method of quantum electrodynamics, the PP total cross section can be obtained (e.g., Akhiezer and Berestetskii, 1965 [4])

$$\sigma_{PP} = \frac{3}{16}\sigma_T(1-\hat{\beta}^2)\hat{\beta}\left[\frac{(3-\hat{\beta}^4)}{\hat{\beta}}\ln\frac{1+\hat{\beta}}{1-\hat{\beta}} + 2(\hat{\beta}^2-2)\right], \tag{2.3}$$

where

$$\sigma_T = \frac{8}{3}\pi r_0^2 \tag{2.4}$$

is the Thomson cross section and r_0 is the classical electron radius.

From the total cross section, the absorption probability per propagation distance for a photon with energy ε moving through an isotropic photon gas can be formulated. Let $n(\omega)$ be the background photon number density per unit energy in the lab frame. In the interval $(\theta, \theta + d\theta)$ there are $(1/2)n(\omega)\sin\theta d\theta$ soft photons interacting with every hard photon, and one obtains

$$\frac{d\tau_{PP}}{dx}(\varepsilon) = \Lambda_{PP}^{-1}(\varepsilon) = \int_{1/\varepsilon}^{\infty} \overline{\sigma}_{PP} n(\omega) d\omega, \tag{2.5}$$

where τ_{PP} is optical depth, Λ_{PP} is the PP mean free path length of the hard photon, with an angle-averaged cross section

$$\overline{\sigma}_{PP} = \frac{1}{2}\int_{-1}^{1-2/s_0} (1-\mu)\sigma_{PP} d\mu. \tag{2.6}$$

Here, $\mu = \cos\theta$ and $s_0 = \varepsilon\omega$. The quantity $(1-\mu)/2$ represents the relative velocity of the soft photon along the direction of propagation of the hard photon. The analytic solution of Eq.(2.6) was found by Gould and Schréder (1967) [5],

$$\overline{\sigma}_{pp} = \frac{3}{8}\sigma_T \left(\frac{1}{s_0}\right)^2 \varphi_{PP}(s_0), \tag{2.7}$$

where

$$\begin{aligned} \varphi_{PP}(s_0) &= \frac{1+\beta_0^2}{1-\beta_0^2}\ln\alpha_0 - \beta_0^2 \ln\alpha_0 - \ln^2\alpha_0 \\ &\quad -\frac{4\beta_0}{1-\beta_0^2} + 2\beta_0 + 4\ln\alpha_0 \ln(\alpha_0+1) - 4L(\alpha_0), \qquad (2.8) \\ \beta_0^2 &= 1 - 1/s_0, \qquad (2.9) \\ \alpha_0 &= (1+\beta_0)/(1-\beta_0), \qquad (2.10) \end{aligned}$$

and $L(\alpha_0)$ is the dilogarithm function,

$$L(\alpha_0) = -\int_0^{\alpha_0} \frac{ln(1-t)}{t} dt, \tag{2.11}$$

which can be written as a series expansion;

$$L(\alpha_0) = \frac{1}{2}\ln^2\alpha_0 + \frac{\pi^2}{12} - \sum_{n=1}^{\infty}(-1)^{n-1} n^{-2} \alpha_0^{-n}. \tag{2.12}$$

The formula in Eq.(2.8) is computationally costly. However, an approximate form is given by (Aharonian, private communication),

$$\begin{aligned} \overline{\sigma}_{PP} &= \frac{3\sigma_T}{2s_0^2}\left[\left(s_0 + \frac{1}{2}\ln s_0 - \frac{1}{6} + \frac{1}{2s_0}\right)\ln(\sqrt{s_0} + \sqrt{s_0-1}) \right. \\ &\quad \left. -\left(s_0 + \frac{4}{9} - \frac{1}{9s_0}\right)\sqrt{1-\frac{1}{s_0}}\right], \end{aligned} \tag{2.13}$$

which requires less CPU time, and still has an accuracy of better than 3%, as evident from Fig. 2.1.

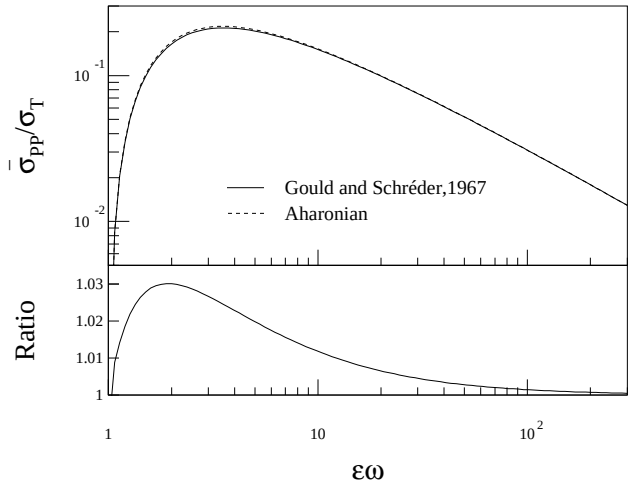

Figure 2.1: The cross section $\overline{\sigma}_{PP}$ as given by Gould&Schréder, 1967 (solid line); i.e., Eq.(2.8), and computed from the approximate formula derived by Aharonian (dashed line); i.e., Eq.(2.13). Both are shown in units of the Thomson cross section σ_T. The approximate formula is accurate to within 3%, as demonstrated in the lower panel.

The mean free path is a key quantity in the numerical simulation, but from a theoretical point of view, especially for PP, the optical depth is more important. For the simple case, when the background photon field $n(\omega)$ is independent of red shift, or when the red shift is too small to affect the background, the optical depth becomes

$$\tau_{PP} = \Lambda_{PP}^{-1} d, \tag{2.14}$$

where $d = cz/H_0$ is the source distance corresponding to a red shift z, H_0 being Hubble's constant[1]. The function $\overline{\sigma}_{PP}$ is strongly peaked, with a maximum at

$$\omega_{max} = 4/\varepsilon, \tag{2.15}$$

and a convenient approximation for the PP optical depth [6, 7] can thus be written

$$\tau_{PP} \approx \frac{\sigma_T}{4} \omega_{max} n(\omega_{max}) d. \tag{2.16}$$

The situation gets more complicated when the photons come from sources located at high red shift, such that the effect of cosmological expansion has to be taken into account. In this case, an observed photon with energy ε_0 corresponds to a photon emitted at red shift z with energy ε_z given by

$$\varepsilon_z = \varepsilon_0 (1 + z). \tag{2.17}$$

The same applies to background photons;

$$\omega_z = \omega_0 (1 + z). \tag{2.18}$$

[1]In this work the Hubble constant has been set to $H_0 = 60$ km/s/Mpc.

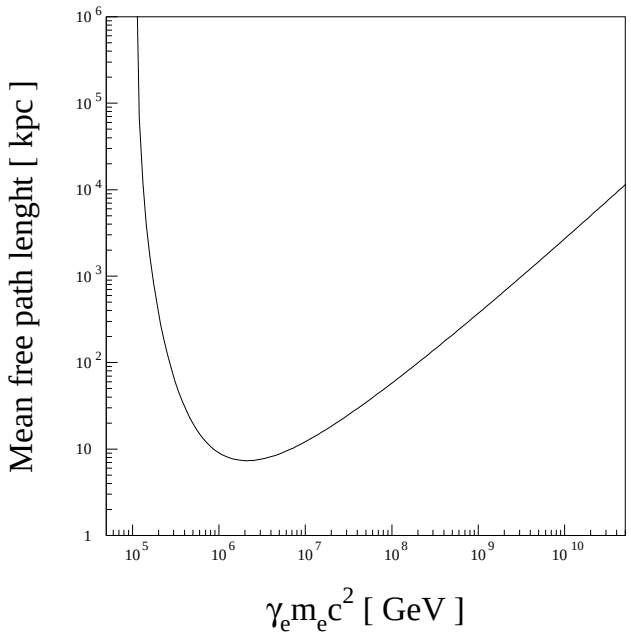

Figure 2.2: The mean free path length of a gamma photon in the 2.7 K microwave background.

A natural consequence of the cosmological expansion is that the volume of the universe was smaller in the past by a factor $(1+z)^{-3}$. Thus, if the background photons were already in place at red shift z and no absorption or re-emission occurs, the background photon field , $n(\omega_z, z)$, as seen by a comoving observer in that epoch becomes

$$n(\omega_z, z)d\omega_z = (1+z)^3 n(\omega_0, 0)d\omega_0. \tag{2.19}$$

The PP optical depth associated with the photons from high red shift sources must include the effects of red shift phenomena. The photon energy ε_z from sources at high red shift z travels through the background photon field $n(\omega_z, z)$ in different red shifts before reaching the observer with energy ε. The PP optical depth, therefore, can be calculated by integrating Eq.(2.5) along the propagation distance $dx = -c\ dt/dz\ dz$:

$$\tau_{PP}(z_s, \varepsilon) \quad = \quad -c \int_0^{z_s} \frac{dt}{dz} dz \int_{1/\varepsilon_z}^{\infty} d\omega_z n(\omega_z, z) \overline{\sigma}_{PP}(\varepsilon_z, \omega_z), \tag{2.20}$$

where dt/dz is the cosmic time-red shift relation. The cosmic time relates with red shift through the time derivative of the scaling factor $\dot{R}(t)$ which is model dependent. In the Friedman cosmological model with cosmological constant $\Lambda = 0$ used in this work the cosmic time-red shift relation.

$$\frac{dt}{dz} = -\frac{1}{H_0(1+z)^2(1+2q_0 z)^{1/2}}. \tag{2.21}$$

Therefore,

$$\tau_{PP}(z_s,\varepsilon) = \frac{c}{H_0}\int_0^{z_s} dz(1+z)^{-2}(1+2q_0z)^{-1/2}\int_{1/\varepsilon_z}^{\infty} d\omega_z n(\omega_z,z)\overline{\sigma}_{PP}(\varepsilon_z,\omega_z), \tag{2.22}$$

where q_0 is the deceleration parameter[2].

Another important function for the model is the resulting $e^{\pm}$ energy distribution. For very different energies between the colliding photons the resulting distribution is given approximately by[3] [8]

$$\begin{aligned}\frac{dN_e(\gamma_e,w,\varepsilon)}{d\gamma_e} &= \frac{3\sigma_T}{32w^2\varepsilon^3}\left[\frac{4\epsilon^2}{(\epsilon-\gamma_e)\gamma_e}\ln\frac{4w(\epsilon-\gamma_e)\gamma_e}{\epsilon} - 8w\epsilon\right.\\ &\left. +\frac{2(2w\epsilon-1)\epsilon^2}{(\epsilon-\gamma_e)\gamma_e} - \left(1-\frac{1}{w\epsilon}\right)\frac{\epsilon^4}{(\epsilon-\gamma_e)^2\gamma_e^2}\right].\end{aligned} \tag{2.23}$$

In Eq.(2.23), $\gamma_e = E_e/m_ec^2$ represents the electron (positron) energy, and $\epsilon = \varepsilon + \omega \approx \varepsilon$ gives the total lab-frame photon energy. The range of γ_e is

$$\frac{\epsilon}{2}\left(1-\sqrt{1-\frac{1}{\epsilon\omega}}\right) \le \gamma_e \le \frac{\epsilon}{2}\left(1+\sqrt{1-\frac{1}{\epsilon\omega}}\right). \tag{2.24}$$

In the current model, the energy difference between the hard and soft photons in the lab frame is greater than 10 orders of magnitude, and Eq.(2.23) is always applicable.

The $e^{\pm}$ spectrum is symmetric about the energy $\epsilon/2$, which is also the minimum point of the function, as shown in Fig. 2.3. One can also see that the larger s_0 is, the more pronounced and the further apart are the maxima of Fig. 2.3. For very large s_0, one of the outcoming particles, e^- or e^+, receives almost all the photon energy (as seen from the lab frame).

2.1.2 Inverse Compton Scattering

To calculate the energy of a photon in the lab frame after scattering on an $e^{\pm}$, the photon energy can be transformed from the lab frame to the $e^{\pm}$ rest frame,

$$\omega' = \gamma\omega(1-\beta\cos\theta), \tag{2.25}$$

where $\gamma = (1-\beta^2)^{-1/2}$, θ is the angle between the electron and photon momenta, and β the $e^{\pm}$ speed in the lab frame. Applying the conservation of four momentum in the $e^{\pm}$ rest frame gives a relation between the photon energy before (ω') and after (ε') scattering;

$$\varepsilon' = \frac{\omega'}{1+\omega'(1-\cos\Theta_1')}. \tag{2.26}$$

Here,

$$\cos\Theta_1' = \cos\theta'\cos\theta_1' + \sin\theta'\sin\theta_1'\cos(\phi'-\phi_1'), \tag{2.27}$$

[2]This work uses $q_0 = 0.5$.

[3]subscript e in the formulas represents electron/positron.

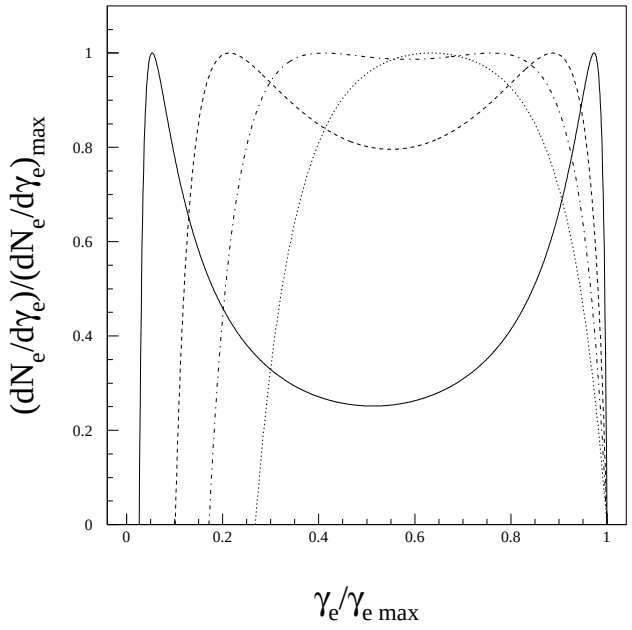

Figure 2.3: Differential spectra of $e^{\pm}$ from $\gamma\gamma$ pair production in different cases: s_0=10 (solid line), $s_0 = 3$ (dashed line), $s_0 = 2$ (dot-dashed line) and $s_0 = 1.5$ (dotted line).

where Θ_1' is the angle between the photon momenta before and after scattering, θ_1' is the angle between the scattered photon and the electron velocity before the scattering, and ϕ' and ϕ_1' are the azimuthal angles of the scattered and incident photon in the rest frame. Transforming back to the lab frame, one obtains

$$\varepsilon = \gamma\varepsilon'(1 + \beta\cos\theta_1'). \tag{2.28}$$

In the special case of a head-on collision, the photon energy gain is given by $\varepsilon_{max} \approx 4\gamma^2\omega$, which is quite large for a photon colliding with a high energy electron. However, it is still small compared with the electron energy; in other words the electron loses a small fraction of its energy in each scattering in the Thomson regime. In the extreme Klein-Nishina regime, on the other hand, the electron loses almost all its energy during one interaction.

In the lab frame, the total cross section for this interaction (e.g., Akhiezer and Berestetskii, 1965[4]) is

$$\sigma_{IC} = \frac{3\sigma_T}{4\chi}\left[\left(1 - \frac{4}{\chi} - \frac{8}{\chi^2}\right)\ln(1+\chi) + \frac{1}{2} + \frac{8}{\chi} - \frac{1}{2(1+\chi)^2}\right], \tag{2.29}$$

where $\chi = 2w\gamma_e(1 - \beta\mu)$.

The collision probability per unit distance for an electron propagating through an isotropic photon gas with density $n(\omega)$ is

$$\frac{d\tau_{IC}}{dx} = \Lambda_{IC}^{-1} = \frac{1}{\beta}\int_0^\infty \overline{\sigma}_{IC} n(\omega) d\omega, \tag{2.30}$$

where τ_{IC} is the $e^{\pm}$ optical depth, Λ_{IC} is respect to IC, and the angle-averaged IC total cross section is

$$\overline{\sigma}_{IC} = \frac{1}{2}\int_{-1}^{1}(1-\beta\mu)\sigma_{IC}d\mu. \tag{2.31}$$

The exact solution for Eq.(2.30) [9, 10] is

$$\overline{\sigma}_{IC} = \frac{3}{8}\sigma_T\left(\frac{1}{\chi_0}\right)^2\varphi_{IC}(\chi_0), \tag{2.32}$$

with

$$\chi_0 = \gamma_e w, \tag{2.33}$$

$$\begin{aligned}\varphi_{IC}(\chi_0) &= F(\chi_0(1+\beta)) - F(\chi_0(1-\beta)) &(2.34)\\ F(\xi) &= -\frac{\xi}{4} + \left(\frac{9}{4}+\frac{1}{\xi}+\frac{\xi}{2}\right)\ln(1+2\xi) + \frac{1}{8+16\xi}\\ &\quad -\frac{3}{8}+\frac{1}{2}\ln^2 2\xi + \frac{\pi^2}{12} - L(-2\xi), &(2.35)\end{aligned}$$

An approximate formula for Eq.(2.32) was derived by Coppi and Blandford (1990) [11]:

$$\overline{\sigma}_{IC} = \frac{3\sigma_T}{8\chi_0}\left[\left(1-\frac{2}{\chi_0}-\frac{2}{\chi_0^2}\right)\ln(1+2\chi_0)+\frac{1}{2}+\frac{4}{\chi_0}-\frac{1}{2(1+2\chi_0)^2}\right]. \tag{2.36}$$

The functional dependence of $\overline{\sigma}_{IC}$ is shown in Fig. 2.4. In the Thomson regime, $\chi_0 \ll 1$, the total cross section is energy independent. In the Klein-Nishina regime, $\chi_0 \gg 1$, the $e^{\pm}$ total cross section is a decreasing function of the $e^{\pm}$ energy; i.e., $\propto \chi_0^{-1}$. The probability per propagation length for IC of an $e^{\pm}$ passing through an isotropic photon gas is shown in Fig. 2.5.

Due to the fact that in the Thomson regime an $e^{\pm}$ loses only a small fraction of its energy in each interaction, one can compute the associated, effective energy loss rate. It is given by (e.g. [12])

$$\frac{d\gamma_e}{dt} = \frac{4}{3}\sigma_T c\gamma_e^2 U_{ph}, \tag{2.37}$$

where U_{ph} is the energy density of the isotropic photon gas

$$U_{ph} = \int_0^{\infty}\omega\ n(\omega)d\omega. \tag{2.38}$$

The mean energy of the scattered photon is

$$\overline{\varepsilon} = \frac{4}{3}\gamma^2\overline{\omega}. \tag{2.39}$$

The spectral distribution of the scattered photons via IC for the isotropic photon gas [13] is

$$\begin{aligned}\frac{dN_\varepsilon}{d\varepsilon} &= \frac{3\sigma_T}{4w\gamma_e^2}\left[1+\frac{x^2}{2(1-x)}+\frac{x}{b(1-x)}-\frac{2x^2}{b^2(1-x)^2}\right]\\ &\quad -\frac{x^3}{2b(1-x)^2}-\frac{2x}{b(1-x)}\ln\frac{b(1-x)}{x}, &(2.40)\end{aligned}$$

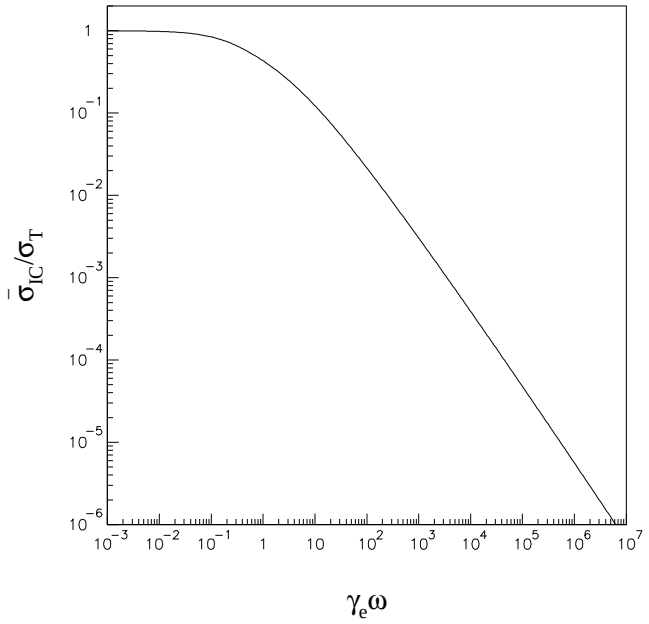

Figure 2.4: The approximation of the angle average IC cross section, $\overline{\sigma}_{IC}$, [11] in Eq.(2.36).

$$\frac{\omega}{\gamma_e} \ll x \leq \frac{b}{1+b} = \frac{\varepsilon_{max}}{\gamma_e}, \tag{2.41}$$

$$x \equiv \frac{\varepsilon}{\gamma_e} \tag{2.42}$$

and

$$b \equiv 4\omega\gamma_e. \tag{2.43}$$

The spectrum of upscattered photons depends only on the parameter b, as illustrated in Fig. 2.6. For small b i.e.; in the Thomson regime, the upscattered photon population is predominantly in the low energy regime, whereas for large b, corresponding to the Klein-Nishina regime, the population is shifted towards high energies.

2.1.3 Synchrotron Radiation

The magnetic field not only confines the cascade $e^{\pm}$ pairs but also induces them to emit the synchrotron photons. It means that the $e^{\pm}$ pairs lose their energies all the time when they travel.

The spectrum of the synchrotron radiation of an $e^{\pm}$ described by as the total emitted power per frequency (see e.g. [12], [14])is

$$\frac{d\gamma_e}{dtd\nu} = \frac{\sqrt{3}e^3 B\sin\alpha}{2\pi mc^2} G(\frac{\nu}{\nu_c}), \tag{2.44}$$

where

$$\nu_c = \frac{3\gamma^2 qB\sin\alpha}{2mc}, \tag{2.45}$$

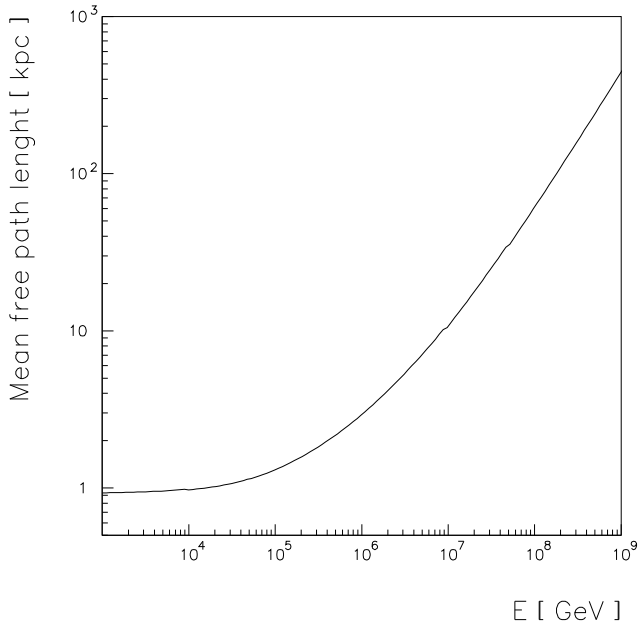

Figure 2.5: Inverse Compton scattering mean free path in 2.7 K black body background photon distribution.

$$G(x) \equiv x \int_x^\infty K_{\frac{5}{3}}(\xi) d\xi, \tag{2.46}$$

and $K_{\frac{5}{3}}(x)$ is modified Bessel function of 5/3 order. The graph of the function $G(x)$ are shown in the Fig.2.7.

The total synchrotron energy loss rate of an $e^{\pm}$ pair that average over all pitch angle (α) is given by

$$\frac{d\gamma_e}{dt} = \frac{4}{3}\sigma_T c \gamma_e^2 U_B, \tag{2.47}$$

where $U_B = B^2/8\pi$ is the energy density of the magnetic field.

2.2 The Physical Model

The $e^{\pm}$ pair halo model which was proposed by Aharonian, Coppi and Völk (1994) [15] concerns the effect of the intergalactic magnetic field on electromagnetic cascades of VHE gamma rays, 1 TeV $< E_{\varepsilon 0} <$ 1 PeV, from extragalactic sources.

The physical basis of the model is schematically shown in Fig. 2.8. The VHE photons are emitted from an extragalactic source. Absorption of these VHE gamma rays via PP with ambient soft photons (e.g., from the cosmic microwave background (CMB) [16] and the cosmic infrared background (CIB) [17, 18]) is substantial on cosmological propagation scales. Only gamma rays with energies greater than several hundred TeV can interact with CMB photons to produce pairs, whereas those with lower energies can produce pairs in collisions with

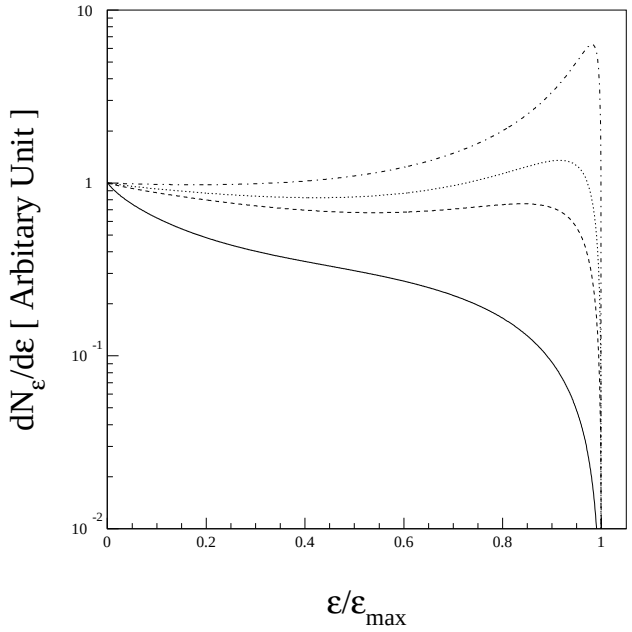

Figure 2.6: Upscattered photon spectral energy distribution in arbitrary units for different cases: b→0 (solid line), b=5 (dashed line), b=10 (dotted line), and b=50 (dot-dashed line).

CIB photons. The number density of the low energy gamma photon population is normally higher than that of the high energy one for a reasonable source spectrum such as a power law. The PP opacity is therefore mainly due to the CIB. Even in the case of a monoenergetic distribution of primary VHE photons at several hundred TeV, the CIB dominates the PP opacity after several cascade generations.

On the other hand, the contribution to the IC opacity is dominated by the CMB, rather than the CIB. The first generation $e^{\pm}$ pairs will interact with soft photons from the same background photon field via IC and produce secondary gamma rays. Almost all soft photons that interact with the $e^{\pm}$ are in the CMB, because it has a much higher number density than the CIB. The IC upscattered gamma photons in the Klein-Nishina regime are absorbed by the CIB, whereas most of the photons from the Thomson regime experience an optically thin background and propagate freely to the observer.

The extragalactic magnetic field plays an important role if it is sufficiently strong, say $10^{-9} < |\mathbf{B}| < 10^{-6}$ G. The gyroradius R_{gyro} of $e^{\pm}$s of energy E_e in this field is about $R_{gyro} = 100$ pc $(E_e/100$ TeV$)(10^{-9}$ G$/|\mathbf{B}|)$. At the same energy, $E_e \approx 100$ TeV, the IC mean free path length $\Lambda_{IC} \approx 1$ kpc, as shown in Fig. 2.9: $R_{gyro} \ll \Lambda_{IC}$. This means that after the $e^{\pm}$s are produced they will gyrate several times before interacting with soft photons via IC, and therefore the secondary gamma rays will be emitted isotropically. In previous cascade models, which do not take into account the effect of the intergalactic magnetic field, the assumption that all cascade particles travel in a straight line to the observer has been applied.

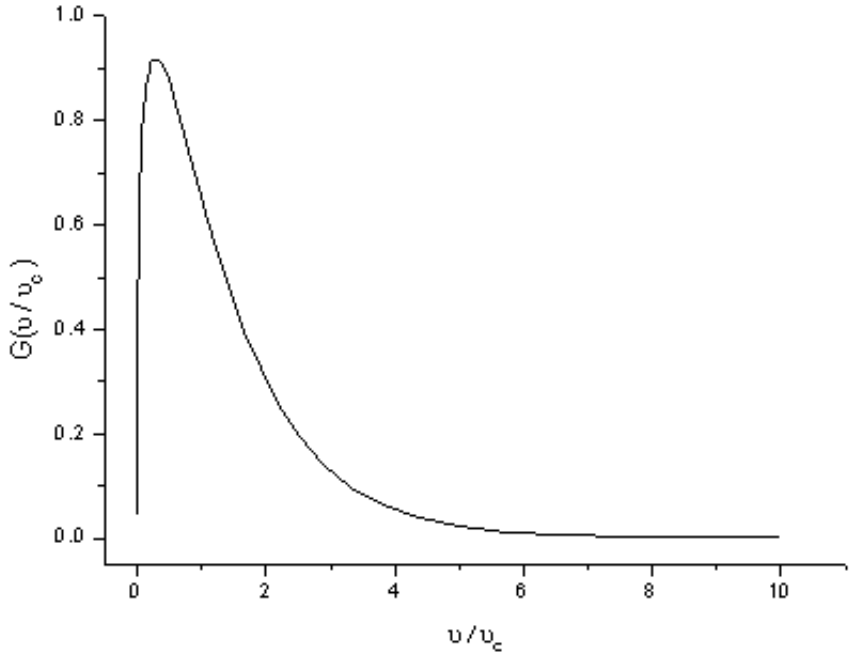

Figure 2.7: Function describing the total power spectrum of synchrotron emiss. The peak of the function is at 0.29 ν_c.

The isotropically upscattered secondary gamma rays with an energy above the PP threshold will produce a new generation of $e^{\pm}$s, which in turn produce still another generation of isotropic secondary gamma rays. The cascade develops until gamma rays of a later generation have an energy less than the threshold energy, $E_{\varepsilon th} = m_e^2 c^4 / E_\omega$. Gamma photons with lower energies do not interact with the background via PP, and therefore travel directly to the observer. Such low-energy gamma photons are generated by the $e^{\pm}$s via IC in the Thomson regime. After many cascade generations, there are a large number of $e^{\pm}$s distributed isotropically around a VHE gamma ray source, and these pairs produce gamma photons which may be detected by an observer.

Due to the fact that the radiation from the pair halo is isotropic, it can be observed from any direction. This fact opens interesting possibilities, in that certain types of VHE gamma ray sources have a highly anisotropic radiation field (e.g., BL Lac galaxies) and can only be observed directly if their jet axis is aligned with the observer. The phenomenon of pair halos might open a new search channel for BL Lac galaxies which have not yet been identified.

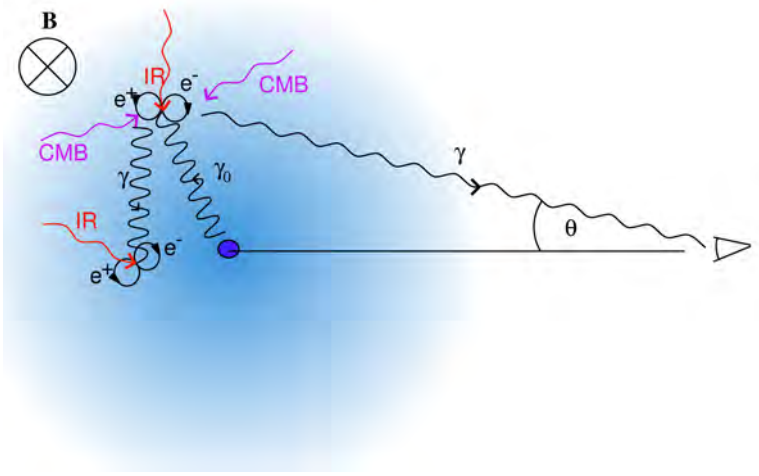

Figure 2.8: Physical picture of $e^{\pm}$ pair halo.

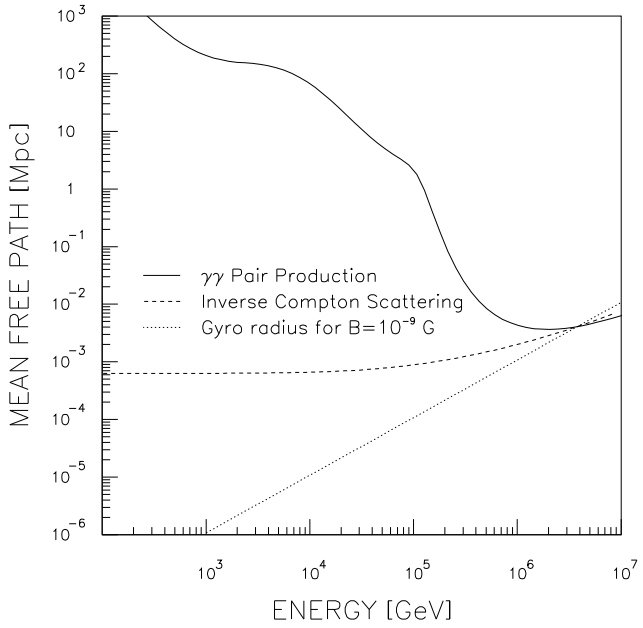

Figure 2.9: The PP and IC mean free path lengths for a specific CBR model, plotted together with the $e^{\pm}$ gyro radius for a magnetic field $|\mathbf{B}| = 10^{-9}$ G.

Chapter 3

Monte Carlo Simulation

From the $e^{\pm}$ pair halo model, the two most important observable quantities are the $e^{\pm}$ pair halo gamma photon energy and angular distribution. To calculate the photon energy distribution from the electromagnetic cascade, most people use the Monte Carlo method and calculation from two transport equations of both $e^{\pm}$s and photons. The transport equation for the $e^{\pm}$s [19] is

$$\begin{aligned}\frac{d\aleph_e(E_e,t)}{dt} &= -\aleph_e(E_e,t)\cdot c\cdot\int dE_\omega n(E_\omega) \\ &\times\int d\mu\frac{1}{2}(1-\beta\mu)\sigma_{IC}(E_e,E_\omega,\mu) \\ &+c\cdot\int dE_e{}'\aleph_e(E_e{}',t)\int dE_\omega n(E_\omega) \\ &\times\int d\mu\frac{1}{2}(1-\beta'\mu)\frac{d\sigma_{IC}}{dE_e{}'}(E_e;E_e{}',E_\omega,\mu) \\ &+c\cdot\int dE_\varepsilon\aleph_\varepsilon(E_\varepsilon,t)\int dE_\omega n(E_\omega) \\ &\times\int d\mu\frac{1}{2}(1-\mu)\frac{d\sigma_{PP}}{dE_e}(E_e;E_\varepsilon,E_\omega,\mu) \\ &+Q_e(E_e,t),\end{aligned} \tag{3.1}$$

where $\aleph_e(E_e,t)$ is the differential number density of $e^{\pm}$s at energy E_e at time t, $n(E_\omega)$ is the differential number density of background at energy E_ω, $Q_e(E_e,t)$ is an external source term for $e^{\pm}$s at energy E_e at time t, μ is the cosine of the interaction angle between the $e^{\pm}$s and the background photons and β is the velocity of the $e^{\pm}$s. Eq.(3.1) describes the changing of the differential number density within interval time dt. The loss rate in the first term is due to $e^{\pm}$s with energy E_ε changing their energies via the IC. The other terms represent the gain rate of the $e^{\pm}$s differential number density due to: $e^{\pm}$s with energy $E_\varepsilon{}'$ change to be E_ε via the IC (the second term), $e^{\pm}$s produced by the PP (the third term), the external $e^{\pm}$ source $Q_e(E_e,t)$ (the last term). For photons the

equation is

$$\begin{aligned}\frac{d\aleph_\varepsilon(E_\varepsilon,t)}{dt} &= -\aleph_\varepsilon(E_\varepsilon,t)\cdot c\cdot\int dE_\omega n(E_\omega) \\ &\times\int d\mu\frac{1}{2}(1-\mu)\sigma_{PP}(E_\varepsilon,E_\omega,\mu) \\ &+c\cdot\int dE_e\aleph_e(E_e,t)\int dE_\omega n(E_\omega) \\ &\times\int d\mu\frac{1}{2}(1-\beta\mu)\frac{d\sigma_{IC}}{dE_\varepsilon}(E_\varepsilon,E_e,E_\omega,\mu) \\ &+Q_\varepsilon(E_\varepsilon,t),\end{aligned} \tag{3.2}$$

where $\aleph_\varepsilon(E_\varepsilon,t)$ is the differential number density of photons at energy E_ε at time t and $Q_\varepsilon(E_\varepsilon,t)$ is an external source term for photons at energy E_ε at time t. The photon differential number density changes because of the loss rate from the PP. Whereas the gain rate from the IC and the external photon source are represented as the second and third term in the right hand side of Eq.(3.2) respectively. Using Eq.(3.1) and (3.2) to compute the energy distribution of the pair halo is much more economical than Monte Carlo simulation in terms of computing time. However, It is clear that the $e^\pm$ pair halo angular distribution can not be gained by using these two transport equations. Another method that can calculate both the energy and angular distribution of the pair halo. It is the solving of the kinetic equations for different generations of particles produced by the cascade [20]. However, this method is only applicable for the pair halo developing in the high magnetic field ($\approx 10^{-6}$ G) region which synchrotron cooling is not negligible. Monte Carlo simulation is the most suitable method for calculating the pair halo angular distribution. The Monte Carlo methods have been defined by Halton (1970) [21]: *the Monte Carlo method is defined as representing the solution of a problem as a parameter of a hypothetical population, and using a random sequence of numbers to construct a sample of the population, from which statistical estimates of the parameter can be obtained.* In the current work, the pair halos were simulated by following all particles, i.e. $e^\pm$s and gamma-photons and calculating all interactions that these particle encounter in the electromagnetic cascades. The Monte Carlo method was used to generate parameters for many distributions that are needed for the simulation. Monte Carlo simulation is arguably the best method, since this allows the most comprehensive analysis for an arbitrary background photon field and primary VHE photon spectrum. This Chapter discusses the Monte Carlo scheme which has been used in the current work.

3.1 Simulation of the Pair Halo

Consider a VHE gamma photon source which is located at red shift z_s while the observer is at red shift 0. The distance between the source and the observer, d_s, equals the coordinate distance, D_c; i.e.,

$$d_s = D_c, \tag{3.3}$$

that can be written as a function of the luminosity distance, D_l, which is more realistic distance,

$$D_c = D_l/(1+z_s). \tag{3.4}$$

The coordinate distance between two objects can be calculated by integrating the line element along the propagation of light which travel from one objects to the other. For the specific cosmology model such as the Friedmann model with cosmological constant $\Lambda = 0$ used in the current work, the coordinate distance can be expressed as [22],

$$D_c = \frac{1}{(1+z_s)} \frac{c}{H_0 q_0^2} \left\{ q_0 z_s + (q_0 - 1) \left[-1 + (2 q_0 z_s + 1)^{1/2} \right] \right\}, \tag{3.5}$$

However, the equivalent expression given by [23],

$$D_c = \frac{1}{(1+z_s)} \frac{c z_s}{H_0} \left[1 + \frac{z_s (1 - q_0)}{(1 + 2 q_0 z_s)^{1/2} + 1 + q_0 z_s} \right], \tag{3.6}$$

is better in order to avoid terms that almost cancel at small $q_0 z_s$. In the case of small z, both Eq.(3.5) and Eq.(3.6) reduces to Hubble's law, $d_s \approx c z_s / H_0$. In the numerical code, there are two conditions which determine when an electromagnetic cascade is stopped:

- The scattering takes place at a distance larger than a maximum value given by $d_c = 10^3 d_s$. This condition ensures that IC scattering beyond the observer which produces radiation returning inward is taken into account.
- The $e^{\pm}$s energy is less than a specified limit, $E_e < E_{e\,min}$.

In principle, the interactions should be simulated until the $e^{\pm}$s have lost all their kinetic energy. For computational reasons, however, this approach is impossible, and the second condition defined above is used. For most of the simulations of the current work, the pair halo photon energy distribution is considered only at energies E_ε above 10 GeV. In order to achieve good statistics for the spectrum down to this value, the minimum electron Lorentz factor $\gamma_{e,\min}$ is then defined according to

$$\begin{aligned} \gamma_{e,\min} &\approx \sqrt{\frac{3}{4} \frac{0.1 \times \overline{E_\varepsilon}_{\min}}{6 \times 10^{-4}\ \mathrm{eV}}} \\ &\approx 10^6 \left(\frac{\overline{E_\varepsilon}_{\min}}{10\,\mathrm{GeV}} \right)^{\frac{1}{2}}. \end{aligned} \tag{3.7}$$

with $\overline{E_\varepsilon}_{\min} = 10$ GeV. In Eq.(3.7), the mean soft photon energy has been taken to be approximately 6×10^{-4}, corresponding to the CMB (see, e.g., [24]), and an empirical constant factor ("0.1" in the formula) has been introduced. For $\overline{E_\varepsilon}_{\min} = 10$ GeV, $\gamma_{e,\min}$ corresponds to an electron energy of $E_{e,\min} \approx 560$ GeV. In Fig. 3.1 the cases of $E_{e,\min} \approx 560$ and 180 GeV are compared. The computational time consumed for the case $E_{e,\min} \approx 180$ GeV is 5 times longer than that for the case $E_{e,\min} \approx 560$ GeV. If one injects one thousand primary gamma photons at energy 100 GeV, the total run time for one simulation is about 30 minutes for the computer hardware available for the current work. The statistical accuracy in the region $E > 1$ TeV in Fig. 3.1 is still low. To improve the statistical accuracy in the extreme high-energy region, the number of primary gamma photons must be increased, unavoidably increasing the computational time. A compromise can be obtained by considering the pair halo SED in the

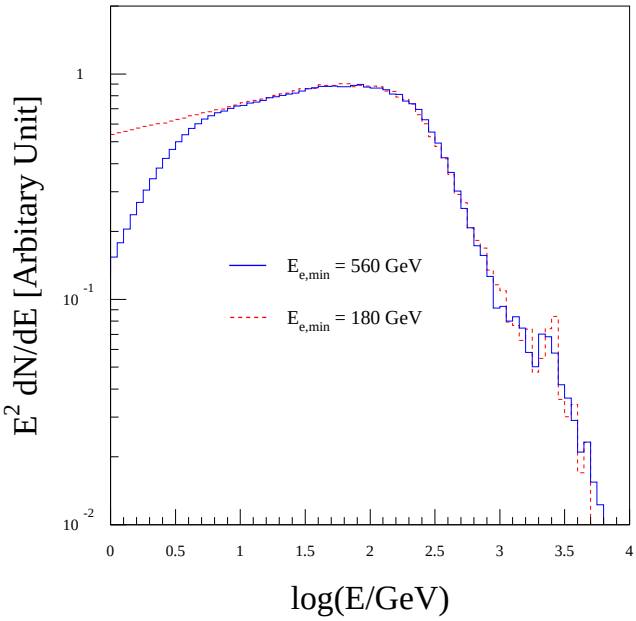

Figure 3.1: The pair halo gamma photon SED computed with $E_{e,\min} \approx 560$ GeV (solid blue line) and with $E_{e,\min} = 180$ GeV (red dashed line).

regions $E < 10$ GeV and $E > 10$ GeV separately. For $E < 10$ GeV, one can use a small number of primary photons but a low value of $E_{e,\min}$, while for $E > 10$ GeV a larger number of primary photons is required, but also a larger value for $E_{e,\min}$ is acceptable. Moreover, the $E > 10$ GeV energy range covers the effective energy region for the next generation imaging atmospheric Cherenkov telescopes system such as H.E.S.S. [25], which is expected to be able to detect pair halos. For each primary gamma photon, the algorithm follows the cascade development through the following procedure:

1. An energy value is given for a primary gamma photon which will start the cascade from a specific source spectrum. Two types of primary photon distributions have been used in the current work. One is monoenergetic,

$$\frac{dN}{dE_\varepsilon} = \delta(E_\varepsilon - E_{\varepsilon 0}), \tag{3.8}$$

and the other is a power law distribution,

$$\frac{dN}{dE_\varepsilon} = \frac{-\alpha + 1}{{E_{\varepsilon 2}}^{-\alpha+1} - {E_{\varepsilon 1}}^{-\alpha+1}} \, {E_\varepsilon}^{-\alpha}, \tag{3.9}$$

where N is a sample number distribution, α is the power index and $E_{\varepsilon 1}$ and $E_{\varepsilon 2}$ are the upper and lower energy limits. The source of the VHE primary gamma photons is located at the origin, (0,0,0).

2. The free path lengths of the gamma photons are generated from the probability distribution

$$\frac{dN}{dr} = \frac{1}{\Lambda_{PP}} \exp(-r/\Lambda_{PP}), \tag{3.10}$$

where Λ_{PP} is a PP mean free path length which depends on the gamma photon energy and the spectrum of the background photon field, as given by Eq.(2.5).

3. The propagation direction for the gamma photon is given in spherical coordinates (r, θ, ϕ). Rather than using θ and ϕ, μ and ϕ are used because of their isotropic distribution in solid angle.

4. The interaction point is computed from the free path and propagation direction. At that point, the PP takes place and produces a $e^{\pm}$ pair. If the point is located out of the considered sphere with radius d_c, this pair will be abandoned and the algorithm considers other $e^{\pm}$s in the memory. If there are no $e^{\pm}$ in the memory, the algorithm will take the actions described in item no. 11. On the other hand, if there is a particle, the program will do as described in item no. 8.

5. A photon to be pair produced is generated. Since the sample space of the background photons that can interact with gamma photons is reduced by the PP cross section, the distribution used is the product of the background photon ($n(z, E_\omega)$) and the angle-averaged PP cross section ($\bar{\sigma}_{PP}$) in Eq.(2.13);

$$\frac{dN}{dE_\omega} = \eta_{PP}(z, E_\varepsilon, E_\omega) = \overline{\sigma}_{PP}(E_\varepsilon, E_\omega) n(z, E_\omega). \tag{3.11}$$

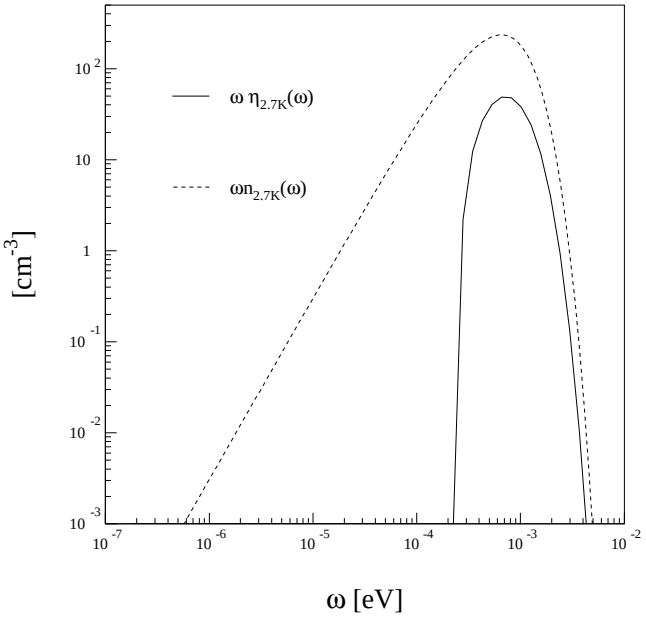

Figure 3.2: Comparison between η_{PP} and n for the case of 2.7 K background with $z = 0$ and gamma photon energy is 100 PeV.

6. Energies for the $e^{\pm}$ pairs are generated. At this stage E_ε and E_ω are known, and the spectrum of the produced $e^{\pm}$ in Eq.(2.23) is used to generate the energies for the $e^{\pm}$ pairs.

7. A particle from the pair, say e^+, is recorded. The parameters that need to be recorded are the particle energy and position. The other particle, e^-, is followed for the next interaction.

   (a) Because the e^- continuously lose its energy via synchrotron radiation, the free path length of the e^- is generated in the more complicated way as described below.

      i. The free path length of the e^- corresponded its present energy is generated from the probability distribution

      $$\frac{dN}{dr} = \frac{1}{\Lambda_{IC}} \exp(-r/\Lambda_{IC}), \tag{3.12}$$

      where Λ_{IC} is a IC mean free path length which depends on the e^- energy and the spectrum of the background photon field, as given by Eq.(2.30).

      ii. Calculate the ratio of the distance that the e^- lose 10 % of its energy to the IC free path. If the ratio is bigger than one, the e^- travels with the IC free path. When the ratio is less than one, the ratio will be compared with a random number generated from a uniform distribution. If the random number is bigger, the e^- travels with 10 %-energy-loss distance. If the random number is smaller, the e^- travels with the length calculated by (see more details in Sec. 3.2)

      $$r = -\Lambda_{IC} \ln \xi, \tag{3.13}$$

      where r is the travelling length, Λ_{IC} is the IC mean free path, and ξ is the uniform random number.

   (b) The e^- gyrates with the free path length and continuously loses its energy via synchrotron radiation with the rate as in Eq.(2.47). The energies and travelling times in every 10%-energy-loss length step are recorded.

   This particle will be abandoned in the record when $E_e < E_{emin}$, after which the program looks for a new one. When there are no more particles in the record, the program will do as described in item no. 11.

8. A photon to be upscattered is generated. The distribution

   $$\frac{dN}{dE_\omega} = \eta_{IC}(z, E_e, E_\omega) = \overline{\sigma}_{IC}(E_e, E_\omega) n(z, E_\omega), \tag{3.14}$$

   is used, with $\overline{\sigma}_{IC}$ from Eq.(2.36). In the model the $e^{\pm}$s gyrate only across a region which is very small relative to the size of the pair halo. Thus, it can be assumed that they remain at the point where they are produced. If the e^- energy is less than the energy limit in Eq.(3.7), the program will abandon this particle and follow the last $e^{\pm}$s in the record. The action taken by the program if there are no $e^{\pm}$ left in the record is discussed in item no. 11.

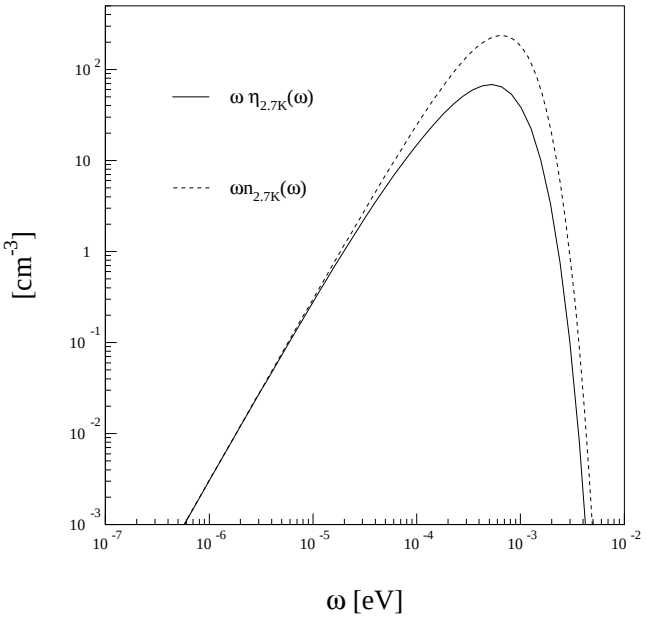

Figure 3.3: Comparison between η_{IC} and n for the case of a 2.7 K background with $z = 0$ and a gamma photon energy of 100 PeV.

9. An upscattered gamma photon is generated. The spectrum of the gamma photons from IC from Eq.(2.40) is used, where the e^- energy and soft photon energy values are already known. After obtaining the gamma photon energy, the energy of the e^- is subtracted.

10. The e^- is recorded, and the program follows the gamma photon. The gamma photon has a higher priority than $e^{\pm}$, in order that the cascade be followed. The gamma photon is followed and the procedure in items no. 2–6 is repeated.

11. When no particles remain in the record, the cascade is aborted and the computations are finished for one primary gamma photon.

During the monitoring of a cascade, several variables have to be computed; e.g., the propagation distances of the particles, the energy of the resulting particles in each interaction, and the soft photon energy w from the background field. The next section discusses the techniques used in the program to compute these variables.

3.2 Random Number Generator

In the current work, the Monte Carlo simulation uses two different random number generators. One is a transformation method, and the other a hit-or-miss method [26].

3.2.1 Transformation Method

In order to generate random numbers from $f(x)$, the transformation method uses a normalized accumulated function of $f(x)$:

$$F(x) = \frac{1}{A}\int_{\acute{x}_{min}}^{x} f(\acute{x})d\acute{x}, \tag{3.15}$$

with a normalization factor

$$A = \int_{\acute{x}_{min}}^{\acute{x}_{max}} f(\acute{x})d\acute{x}. \tag{3.16}$$

The function $F(x)$ is a monotonically increasing function in the range 0 to 1. When a random number ξ has been chosen from a uniform probability distribution on the interval (0,1), the variable x can be calculated. In the case of $F(x)$ being an analytically invertible function, one can find x from

$$x = F^{-1}(\xi). \tag{3.17}$$

However, if $F(x)$ cannot be inverted, one can tabulate $F(x)$ and x and find the x-value corresponding to ξ by interpolation. This method is used to generate the free path length of the particles, with a probability density which attains an exponential form,

$$f(x) = \Lambda^{-1}e^{-x/\Lambda}. \tag{3.18}$$

The normalized accumulated distribution is

$$F(x) = (1 - e^{-x/\Lambda}), \tag{3.19}$$

and the free path length can be produced by inverting the normalized accumulated function

$$x = -\Lambda \ln \xi, \tag{3.20}$$

where Λ is the free path length from Eq.(2.6) for PP and Eq.(2.30) for IC. The transformation method is computationally efficient in one-dimensional problems, especially when $F(x)$ is an invertible function. There are, however, disadvantages of the method in multidimensional or many-variable problems, the reason being that in these cases the accumulated distribution cannot generally be inverted with respect to every variable. Typically, interpolating between tabulated values is practical only for functions with up to two variables.

3.2.2 hit-or-miss Method

The hit-or-miss method is the most simple technique for generating random numbers, provided there is a distribution $f(x)$ from which random numbers α can be taken. The procedure is as follows:

1. Two random numbers, α and ξ, within the intervals (x_{min}, x_{max}) and (y_{min}, y_{max}), are independently obtained from a uniform probability distribution.

2. The *hit-or-miss condition* is checked: if $\xi \leq f(\alpha)$ then α is accepted (hit), but if $\xi > f(\alpha)$ then α is rejected (miss).

The distribution of the accepted α will have the same shape as $f(x)$. The necessary parameters are x_{min}, x_{max}, y_{min}, and y_{max}. However, in practice, at least in this simulation, only y_{max} is an unknown parameter. Hence, in this simulation before the program generates the random number from a distribution function $f(x)$ the program has to find the maximum value of $f(x)$, y_{max}. The efficiency of the hit-or-miss technique depends on

$$p = \frac{\text{area under } f(x)}{\text{area of sample space}} = \frac{\int_{x_{min}}^{x_{max}} f(x)dx}{(x_{max} - x_{min}) \times (y_{max} - y_{min})}. \tag{3.21}$$

When $p \approx 1$, the area under the curve $f(x)$; i.e., the "hit" area, is nearly the same as the sample space area. Most of the sample in the sample space is in the hit area. In contrast, if $p < 0.5$, most of the sample is in the "miss" area, and the program has to generate random numbers many times to get a satisfactory value. One advantage of this technique, and the main reason that it was chosen for the current work, is that it can be applied for many-parameter problems, such as is the case for the pair halo model. In PP, the hit-or-miss technique is applied for two tasks. One is to generate the energy of the pair produced $e^{\pm}$ from Eq.(2.23), which depends on two parameters (γ and w) and one variable (E_{ee}). From Fig. 2.3, it is seen that this method is very efficient when s_0 is a low value. Fortunately, most of the PP processes in the pair halo model concerns such cases. The other task is to generate soft photons from the background photon distribution. For this task, the methodology that was suggested in [10] has been applied, where the soft photons are generated from a modified background photon distribution, $\eta_{PP}(E_\varepsilon; w)$ in Eq.(3.11). Here, $p < 0.5$, so this technique is not particularly efficient. However, because the program deals with a number of PP which is much lower than that of IC, it is still acceptable to use this technique for generating soft photons. In IC, the hit-or-miss technique is applied only in order to generate the energy of the upscatter gamma photons from Eq.(2.40). As seen from Fig. 2.6, this method is not very efficient in the Klein-Nishina regime, but it is quite good in the Thomson regime, especially in the case of b < 10. Fortunately, most of the IC processes in the cascade are within the last regime. The hit-or-miss method is not appropriate for generating the IC interacting soft photons from the modified background photon field η_{IC}, as in Eq.(3.14). This is partly due to the fact that $p \ll 1$ for the modified background photon distribution, but also because most of the interactions that occur in the program are IC in the Thomson regime. Thus, the computational demands here are high. The hit-or-miss method together with the comparison function technique; e.g., [27], is needed to solve this problem. Such a technique can be used to improve the random number generated from the hit-or-miss method, especially in the case of $p \ll 1$. The idea is to apply a transformation method to generate random numbers α from a distribution function $g(x)$ that has the following properties:

1. $g(x) > f(x)$ for all x
2. $g(x)$ is an integrable function for which the accumulated distribution invertible.

When α is generated, $g(\alpha)$ will be set equal to y_{max}. Then isotropically distributed random numbers ξ from (y_{min},y_{max}) are generated. The *hit-or-miss*

condition is applied to ξ in order to select α from the distribution $f(x)$. The efficiency of this technique depends on how close the function $g(x)$ is to $f(x)$. This technique can be modified for application to problems that have many parameters by finding an integrable function $g(x)$ which satisfies $g(x) > f(x_1, x_2, ..., x_n; x)$ for all x and all parameters $x_1, ..., x_n$.

3.3 Collecting Data

Two important data needed to be recorded in the simulation are angular distance from the central source and the synchrotron emission time distribution, $dt/dE = T(E)$, of all cascading $e^{\pm}$s. Since the $e^{\pm}$s lose their energy via synchrotron radiation during gyration, their energies needed to be recorded in every 10%-energy-loss length step (as described in item 7 page 22) and weighted by the emission time in that length step. The distribution of the synchrotron energy is calculated by

$$\frac{dE}{d\nu} = \int \frac{\sqrt{3}e^3 B \sin\alpha}{2\pi mc^2} G(\frac{\nu}{\nu_c}) T(E) dE. \tag{3.22}$$

The main assumption used to obtain the pair halo energy flux is that the cascade is in a steady state, implying a constant primary VHE photon flux from the central source. The steady-state has been used in several previous works on cascades; e.g., [9, 10, 28]. The observed pair halo gamma-ray luminosity is then proportional to the luminosity of the VHE primary gamma photons, and one obtains

$$L_0 = kE_s, \tag{3.23}$$

where k is a constant used to convert energy to luminosity, and E_s is total energy of the VHE primary gamma photons. During a cascade, the total primary gamma photon energy is converted into four forms: pair halo gamma photon energy E_{gamma}, pair halo synchrotron photon energy E_{syn}, pair energy E_e, and survival primary gamma photon energy E'_s;

$$E_s = E_{\mathrm{gamma}} + E_{\mathrm{syn}} + E_e + E'_s. \tag{3.24}$$

The luminosity of the pair halo synchrotron photons,

$$L_{\mathrm{syn}} = kE_{\mathrm{syn}}, \tag{3.25}$$

is related to the source luminosity via

$$\frac{L_{\mathrm{syn}}}{L_0} = \frac{E_{\mathrm{syn}}}{E_s}. \tag{3.26}$$

From this relation, the pair halo luminosity can be found, and the pair halo flux can be calculated via

$$F_{\mathrm{syn}} = \kappa E_{\mathrm{syn}} \tag{3.27}$$

where

$$\kappa = \frac{\mathrm{L}_0}{\mathrm{E}_s 4\pi d_s^2}. \tag{3.28}$$

The factor κ is used to convert the energy into energy flux.

A specific strategy has been adopted for collecting angular distances from the simulation, in order to reduce the number of primary gamma photons; i.e.,

computation time. The strategy is based on the fact that the halo is spherically symmetric, and thus observing from any direction from a given distance yields the same picture. An observer located at a sphere with a radius equal to the distance between the VHE gamma source and the observer, d_s, is formed, with the VHE photon source located at the center of the sphere. Every time that an $e^{\pm}$ is generated, a virtual ray is generated randomly. The ray will cross the observer sphere somewhere and make an angle, θ, to the normal of the sphere at the crossing point. The angle θ is interpreted as the angular distance from the source of the $e^{\pm}$. As shown in Fig. 3.4, the normal vectors on the observer sphere are always in the same direction as the line of sight. Therefore, the angle between the photon direction of propagation and the normal vector can be interpreted as the angular distance of the observed gamma photons from the VHE source. If synchrotron photons, produced at $\mathbf{r}_0$ and propagated in the

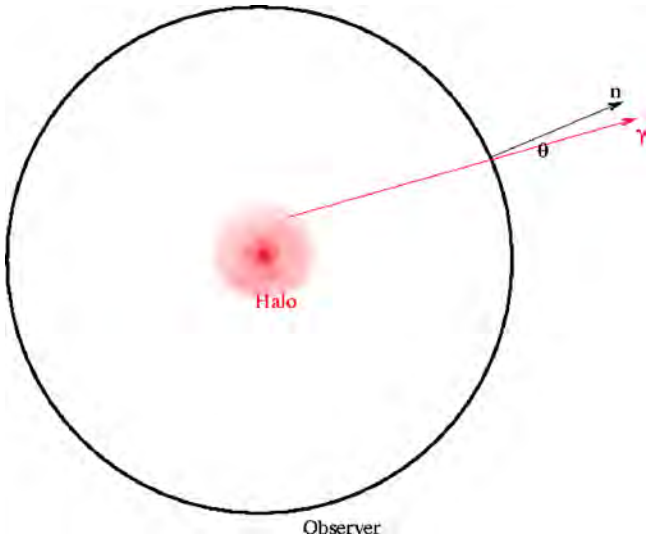

Figure 3.4: Geometry picture shows how to collect data from the simulation.

direction $\hat{\mathbf{k}}_\gamma$, cross the observer sphere (with radius R), the condition

$$(\mathbf{r}_0 \cdot \hat{\mathbf{k}}_\gamma)^2 + R^2 - r_0^2 > 0 \tag{3.29}$$

has to be satisfied. If Eq.(3.29) is not satisfied, the synchrotron photons never cross the observer sphere. Otherwise, the distance between the point where the gamma photons were produced and the crossing point can be calculated from

$$d = -(\mathbf{r}_0 \cdot \hat{\mathbf{k}}_\gamma) \pm \sqrt{(\mathbf{r}_0 \cdot \hat{\mathbf{k}}_\gamma)^2 + R^2 - r_0^2}. \tag{3.30}$$

For $d < 0$, the synchrotron photon propagates in the direction opposite to $\hat{\mathbf{k}}_\gamma$, and this case is rejected otherwise the real crossing point can be calculated by

$$\mathbf{r}_1 = \mathbf{r}_0 + d\,\hat{\mathbf{k}}_\gamma. \tag{3.31}$$

At this point the angle θ is given by

$$\cos\theta = \frac{\mathbf{r}_1 \cdot \hat{\mathbf{k}}_\gamma}{|\mathbf{r}_1|}. \tag{3.32}$$

Note that because the probability density in θ-space is proportional to $\cos\theta$, the histogram in this case has to be weighted by the factor $|\cos^{-1}\theta|$.

Chapter 4

Results and Discussion

Two observed quantities that we can observed from a pair halo in X-ray are spectral energy distribution (SED) and distribution of angular distance from the central source. In this chapter, we used the distributions from many situations to learn the nature of X-ray pair halo. All of the distributions presented here were from the pair halos observed within 0.1° and their central sources emitted monoenergetic gamma-ray spectrum with gamma luminosity of 10^{45} erg/s. The common conditions we used in these simulations are: The intrinsic gamma-ray energy was 500 TeV, the red shift was $z = 0.129$[1] corresponding to 750 Mpc (or about 2.3 billion light years), the inter galactic magnetic field was 1 μG, and the CIB model from Primack's group [29] shown in Fig. 4.1, unless state otherwise.

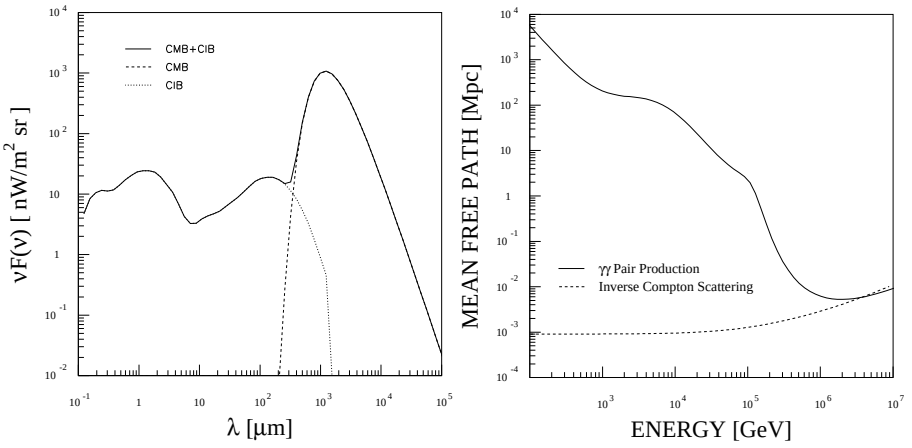

Figure 4.1: Left panel: (a) The background photon field at z=0.129. The CIB component is from [29]. Right panel: (b) The mean free path length of gamma photons with respect to PP, and of $e^{\pm}$ with respect to IC, given the background photon field.

[1] The red shift of H1426, one of the promising candidate pair halo sources.

X-ray pair halos from difference primary gamma-ray energies

Since the intrinsic gamma-rays from the central source initiated the electromagnetic cascades to produce $e^{\pm}$s that radiated the synchrotron photons, the energy of the gamma-ray is obviously affect on the X-ray pair halo. The results in Fig. 4.2 and 4.3 show how the SEDs and the angular distributions responded to the intrinsic gamma energy.

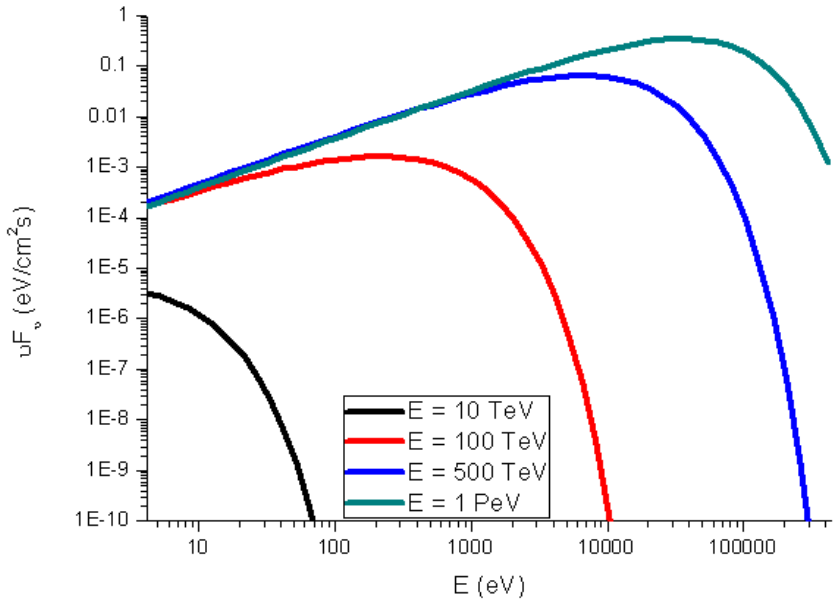

Figure 4.2: Spectral energyt distributions of the pair halo synchrotorn with difference primary gamma-ray energyies

One will see in the Fig.4.2 that the higher intrinsic gamma energies, the higher maximum energies and fluxes in higher energy bands. On the other hands, in lower energy band the X-ray flux is not affected. This phenomena can be explained that since the energies of the cascaded $e^{\pm}$ depend on the energy of their parent gamma-rays. The higher energy gamma-rays produced higher energy $e^{\pm}$s, which in turn radiate more powerful synchrotron photons. At the same time, because the higher energy $e^{\pm}$s lost their energies faster than the lower one (see Eq.(2.47))the synchrotron SED peaked at higher energy band.

Angular distribution of the pair halos from difference intrinsic gamma-ray energies are presented in Fig.(4.3). One will see that the angular distribution peak at the first bin of the histogram. It is interpreted that most of the pair halo flux contain at the center and gradually fainter radially. The results from the figure show that the X-ray pair halos are more centrally peak when the energy of the intrinsic gamma-rays is higher. It is interesting that the angular distribution sensitive to the intrinsic gamma-ray energy between 100 to 500 TeV. This fact

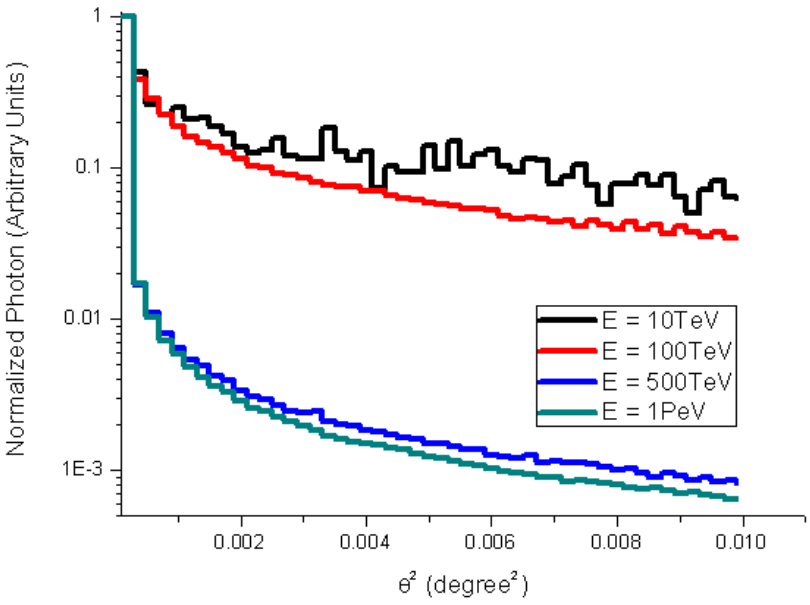

Figure 4.3: Angular distributions of the pair halo synchrotorn with difference primary gamma-ray energies

can be explained that the PP mean free path of the intrinsic gamma-rays with energy between 100 - 500 TeV is the same order as the length of angular size 0.1°. What we observed in this angular size is mainly influence by the first generation $e^{\pm}$ pairs.

X-ray pair halos in difference Magnetic filed strength media

All previous works on the pair halos [15, 30] neglected the radiation from the synchrotron radiation and considered only gamma-rays from IC. Therefore, this is the good opportunity to learn how magnetic field affect on the pair halos especially in X-ray band.

The SEDs presented in Fig. 4.4 show how the X-ray pair halos respond to the magnetic field strength. The synchrotron energy flux of the pair halos increase in all energy bands by order two of the magnetic field strength whereas the maximum energy increase by order one, which can be observed by consider the peaks of the SEDs in difference magnetic strengths. This fact corresponding to Eq.(2.47) and Eq.(2.45) that described the synchrotron radiated power and maximum frequency as functions of magnetic field strength.

The angular distributions of the synchrotron photons from pair halos in difference magnetic field strengths are shown in Fig. 4.5. It is very interesting to see that the distributions get less centrally peak quite fast when the magnetic fields reached 1 μG, but it get more centrally peak again and even faster if the

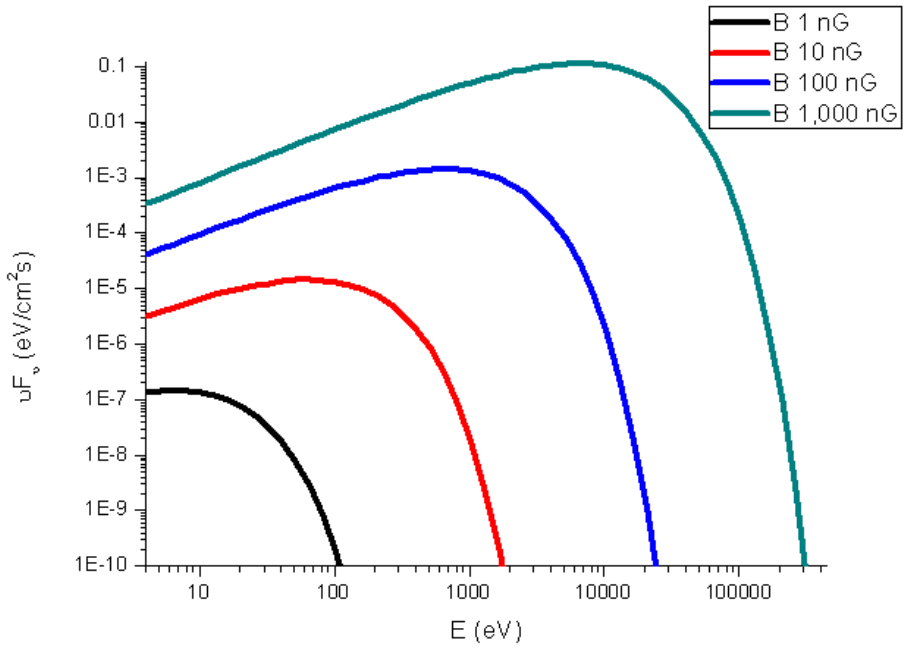

Figure 4.4: Spectral energyt distributions of the pair halo synchrotorn with difference magnetic field strengths

magnetic field stronger than 1 μG. The results can be interpreted that when the magnetic field is weak, say 1 nG, the $e^{\pm}$s lose very small energy via synchrotron radiation, but mostly via IC that proceed the electromagnetic cascades. When the magnetic field get stronger synchrotron radiation get more pronounced and more comparable to the IC. The $e^{\pm}$s lose most of their energy via synchrotron radiation when the magnetic field is stronger than 1 μG. As the result, the $e^{\pm}$s do not have enough energy to continue the electromagnetic cascades further from the central source.

The results we got from the simulations show that observing X-ray pair halos can provide us the information of the ambient magnetic fields and the intrinsic gamma-rays maximum energy. Especially the magnetic fields, the information from X-ray pair halos at difference central source red shifts will show how the structure of the magnetic filed of the Universe develop after the Big Bang. However, observing the X-ray pair halos is still be very challenging for X-ray astronomy since X-ray pair halo fluxes are much lower than the sensitivities of the present X-ray observatories such as *Chandra*, *XMM-Newton* and *Suzaku*. That problem might be solved by using stack of X-ray data from the candidate sources to increase X-ray flux.

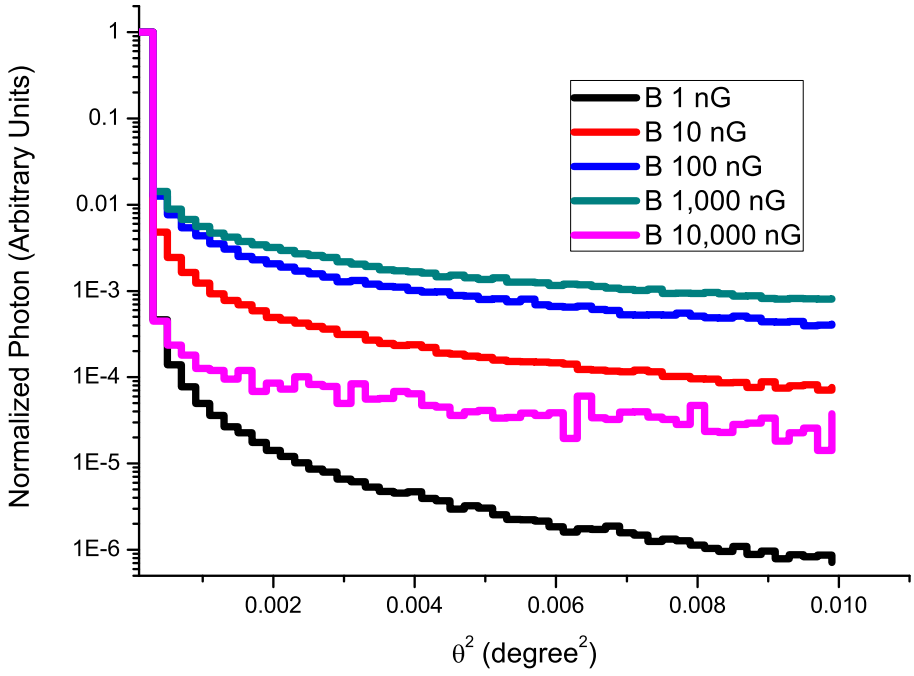

Figure 4.5: Angular distributions of the pair halo synchrotorn with difference magnetic field strengths

Bibliography

[1] V. S. Berezinsky and V. A. Kudriavtsev. On the diffuse gamma radiation at ultra-high energies, $E_\gamma \gtrsim 10^{14}$ eV. *ApJ*, 349:620–624, 1990.

[2] R. J. Protheroe and T. Stanev. Electron-photon cascading of very high energy gamma-rays in the infrared background. *MNRAS*, 264:191–200, 1993.

[3] P. S. Coppi and F. A. Aharonian. Constraints on the very high energy emissivity of the universe from the diffuse GeV gamma-ray background. *ApJ*, 487:L9–L12, 1997.

[4] A. I. Akhiezer and V. B. Berestetskii. *Quantum Electrodynamics*. Interscience Publishers, New York, 1965.

[5] R. J. Gould and G. Schréder. Pair production in photon-photon collisions. *Phys. Rev.*, 155:1404–1407, 1967.

[6] K. Herterich. Absorption of gamma rays in intense x-rays sources. *Nature*, 250:311–312, 1974.

[7] F. A. Aharonian et al. The time averaged TeV energy spectrum of mkn501 of the extraordinary 1997 outbust as measured with the stereoscopic cherenkov telescope system of hegra. *Astron. Astrophys.*, 349:11–28, 1999.

[8] F. A. Aharonian, A. M. Atoyan, and A. M. Nagapetian. Photoproduction of electron-positron pairs in compact x-rays sources. *Astrofizika*, 19:187–194, 1983.

[9] F. A. Aharonian, V. G. Kirillov-Ugryumov, and V. V. Vardanian. Formation of relativistic electron-photon showers in compact x-ray sources. *Astrophys. Space Sci.*, 115:201–225, 1985.

[10] R. J. Protheroe. Effect of electron-photon cascading on the observed energy spectra of extragalactic sources of ultra-high-energy γ-rays. *Mon. Not. R. astr. Soc*, 221:769–788, 1986.

[11] P. S. Coppi and R. D. Blandford. Reaction rates and energy distributions for elementary processes in relativistic pair plasmas. *Mon. Not. R. astr. Soc.*, 245:453–469, 1990.

[12] G. R. Blumenthal and R. J. Gould. Bremsstrahlung, synchrotron radiation, and compton scattering of high-energy electrons traversing dilute gases. *Rev. Mod. Phys.*, 42:237–269, 1970.

[13] F. A. Aharonian and A. M. Atoyan. Compton scattering of relativistic electrons in compact x-ray sources. *Astrophys. Space Sci.*, 79:321–336, 1981.

[14] George B. Rybicki and Alan P. Lightman, editors. *Radiative Processes in Astrophysics*. Wiley-VCH Verlag GmbH, Weinheim, Germany, May 1985.

[15] F. A. Aharonian, P. S. Coppi, and H. J. Völk. Very high energy gamma rays from active galactic nuclei: Cascading on the cosmic background radiation field and the formation of pair halos. *ApJ*, 423:L5–L8, 1994.

[16] R. J. Gould and G. Schréder. Opacity of the universe to high-energy photons. *Phys. Rev. Lett.*, 155:252–254, 1966.

[17] J. Wdowczyk, A. Tkaczyk, and A. W. Wolfendale. *J. Phys. A.*, 5:1419, 1972.

[18] F. W. Stecker, O. C. De Jager, and M. H. Salamon. *ApJ*, 390:L49, 1992.

[19] S. Lee. Propagation of extragalactic high energy cosmic and γ rays. *Phys. Rev. D.*, 58:043004, 1998.

[20] D. Khangulyan. *Space structure and spectrum of radiation of some astrophysical objects*. PhD thesis, Moscow Engineering Physics Institute, 2003.

[21] J. H. Halton. A retrospective and prospective survey of the Monte Carlo method. *Siam Rev.*, 12:1–63, 1970.

[22] W. Mattig. Über den Zusammenhang zwischen Rotverschiebung und scheinbarer Helligkeit. *Astron. Nach.*, 248:109, 1958.

[23] J. Terrell. The luminosity distance equation in fiedmann cosmology. *Am. J. Phys.*, 45:869–867, 1977.

[24] P. V. Ramana Murthy and Wolfendale. *Gamma-ray astronomy*. Cambridge University Press, England, first edition, 1986.

[25] A. K. Konopelko. Stereo imaging of the VHE γ-rays with HEGRA & H.E.S.S. In F. A. Aharonian and H. J. Völk, editors, *High Energy Gamma-ray Astronomy*, pages 569–573, 2000.

[26] F. James. Monte carlo theory and practice. *Rep. Prog. Phys.*, 43:1145–1189, 1980.

[27] W. H. Press, S. A. Teukolsky, W. T. Vetterling, and B. P. Flannery. *Numerical Recipes in C*. Cambridge university press, New York, second edition, 1994.

[28] A. A. Zdziarski. Saturated pair-photon cascades on isotropic background photons. *ApJ*, 335:786–802, 1988.

[29] J. R. Primack, R. S. Somerville, J. S. Bullock, and J. E. G. Devriendt. Probing galaxy formation with high energy gamma-rays. In F. A. Aharonian and H. J. Völk, editors, *High Energy Gamma-Ray Astronomy*, 2000.

[30] A. Eungwanichayapant and F. Aharonian. Very High Energy Gamma Rays from $e^{\pm}$ Pair Halos. *International Journal of Modern Physics D*, 18(06):911, July 2009.

Output

- Papers

  A. Eungwanichayapant, W. Maithong and D. Ruffolo. Synchrotron Radiation from $e^{\pm}$ Pair Halos, *ApJ*, in preparation.